Roman KUZIAK, Zofia KANIA

Instytut Metalurgii Żelaza

Hans ROELOFS

Swiss Steel A.G.

Władysław ZALECKI, Krzysztof RADWAŃSKI, Ryszard MOLENDA

Instytut Metalurgii Żelaza

ADJUSTMENT OF BAINITIC HARDENABILITY TO MEET CRITICAL REQUIREMENTS FOR STEEL PRODUCTS NEW APPLICATIONS

This paper presents the results of the investigation aimed at identification of the optimum conditions for obtaining the maximum volume fraction and stability of retained austenite against mechanical loading in commercial bainitic steel produced by Swiss Steel AG. The volume fraction and stability of this phase is crucial for achieving the advantageous effect of transformation induced plasticity caused by its transformation to martensite during deformation (TRIP effect). The investigation has shown that in order to achieve the optimal TRIP effect in the investigated steel, the decomposition of austenite into bainite should occur in the temperature range 430÷370°C. The range of temperatures of the bainitic transformation in case of continuous cooling of bars depends on their radius. For the smallest diameters, below 6 mm, the bainitic transformation start temperature is close to M_s temperature. However, the occurrence of recalescence effect slows down the rate of cooling which prevents against the martensite formation.

Key words: bainitic hardenability, bainitic steel, phase transformations

REGULACJA HARTOWNOŚCI BAINITYCZNEJ W CELU SPEŁNIENIA KRYTYCZNYCH WYMAGAŃ DLA NOWYCH ZASTOSOWAŃ WYROBÓW STALOWYCH

Artykuł prezentuje wyniki badań, których celem było określenie optymalnych warunków dla uzyskania maksymalnej zawartości austenitu resztkowego oraz jego odpowiedniej stabilności na obciążenia mechaniczne w komercyjnej stali bainitycznej produkowanej przez firmę Swiss Steel AG. Udział oraz stabilność decyduje o korzystnym wpływie przemiany tej fazy indukowanej odkształceniem (z ang. efekt TRIP) na właściwości mechaniczne i użytkowe wyrobów stalowych. Badania pokazały, że dla optymalizacji efektu TRIP w badanej stali, przemiana fazowa austenitu w bainit powinna zachodzić przy temperaturach z przedziału 430÷370°C. Zakres temperatur, w których zachodzi przemiana bainityczna w warunkach ciągłego chłodzenia prętów zależy od średnicy pręta. Dla najmniejszych średnic, poniżej 6 mm, przemiana zachodzi z austenitu silnie przechłodzonego, zaś temperatura początku przemiany przybliża się do temperatury Ms. Jednak efekt rekalescencji zmniejsza szybkość spadku temperatury, co przeciwdziała tworzeniu się martenzytu w strukturze stali.

Słowa kluczowe: hartowność bainityczna, stal bainityczna, przemiany fazowe

1. INTRODUCTION

Due to a wide range of mechanical properties, bainitic steels are good candidate for many applications, for example in automobile and power generating industries, as well as in the production of premium rails or for armoured plates with outstanding ballistic properties [1]. In order to obtain a mass-tailored combination of mechanical and functional properties, the complex microstructure of these steels must be carefully adjusted in the production process. This can be done in several ways, including hardenability design through the adoption of a proper chemical composition, developing a proper austenite microstructure shaped during thermomechanical processing (recrystallized versus non-recrystallized austenite, grain size) and applying the relevant cooling rates after thermomechanical treatment. In industrial practice, all these methods must be applied in a properly balanced way. One of the promising direction of bainitic steels development involves the utilisation of the TRIP effect to improve their properties, including fatigue strength, wear and creep resistance.

Next generation of car components is expected to be more miniature following weight reduction. High strength steels are than welcome in automobile indu-

stry. On the other hand, due to larger internal stresses they might be more sensitive to internal defects limiting the lifetime of the component. Therefore, car component producers ask not only for high strength level combined with high ductility but also for "damage resistant microstructures". The TRIP-assisted bainitic steels have unique property combinations which help to fulfil these future demands. In particular, retained austenite in the bainitic microstructure is expected to suppress the crack propagation and thus to improve the fatigue strength.

The paper demonstrates the capability of steel grades commercially produced at Swiss Steel to develop the TRIP effect in conventionally hot rolled wire rods and bars. Subsequent production steps like peeling, straightening, stress-relieving will also be taken into account.

The TRIP effect is controlled by the amount and mechanical stability of the retained austenite, as well as the dispersion of this phase in the microstructure. Although, the stability of austenite is influenced mostly by its carbon content, it may be affected by many factors including the hardenability of a steel, state of austenite microstructure prior to transformation, and finally, applied cooling conditions or temperature/time of isothermal holding [2, 3].

Within the present work, conditions for the optimisation of TRIP effect in a commercial bainitic steel were identified. The investigation was done on laboratory cast. The bainitic hardenability concept was applied in connection with dilatometric studies and experiment conducted in Gleeble 3800 thermal-mechanical simulator and experiments of continuous bar cooling from temperatures of austenite stability.

2. CHARACTERIZATION OF BAINITIC MICROSTRUCTURES

In this paper, bainite is referred to as the structure that forms under non-equilibrium conditions where ferrite (bainitic ferrite) is a leading phase and the rest is carbon enriched austenite and/or constituents formed as a result of decomposition of remaining austenite after bainitic ferrite formation. It can be obtained in the temperature range where carbon diffusion is slow enough to prevent transformation of austenite into ferrite and pearlite, and at the same time allowing avoiding the martensite formation. The bainitic structures can be obtained either during the continuous cooling or during isothermal holding. Although there have been many researches, e.g. [4–6], focussing on the nature of bainitic transformation in steels, its mechanism has not been fully understood so far.

Based on experimental results, two opposite mechanism of bainitic transformation have been considered and divided the scientists from all over the world, namely:
– displacive as in the case of martensite, and
– diffusional – analogy to the Widmanstätten (ledge mechanism).

Displacive mode of transformation precludes that the substitutional and solvent atoms do not change their position over distance greater than atomic spacing. The bainitic ferrite/austenite interface must have glissile nature as during the martensitic transformation.

The opposite – diffusional – mode of bainitic transformation is based upon the assumption that bainite forms as a result of diffusional transformation involving so called ledge mechanism. The surface of the interface has an incoherent (disordered) structure.

Generally, it is agreed that two stages are involved in the bainitic microstructure formation, namely:
– $\gamma \rightarrow \gamma_{ce} + \alpha_b$
– $\gamma_{ce} \rightarrow \alpha_b +$ *iron carbides*
where: γ_{ce} stands for carbon enriched austenite and α_b for bainitic ferrite.

Thus, early classifications of bainitic structure distinguished two morphological types, namely, upper and lower bainite and the displacive mechanism of their formation is schematically shown in Fig. 1. According to this mechanism, the carbon supersaturated bainitic ferrite plate (called sub-unit) is formed first via displaceive mode. After this event, carbon diffuses to surrounding austenite. The diffusion process is fast at high temperatures of transformation and slow at lower temperatures. This is reflected in morphological features of iron carbides formed during further decomposition of carbon enriched austenite. Accordingly, the bainitic ferrite laths boundaries are the preferential sites for the cementite nucleation in the case of upper bainite. On the contrary, inter laths nucleation of iron carbides is typical in the case of lower bainite, and the cementite particles are aligned at the angle close to 60° with respect to the plate longitudinal plate direction.

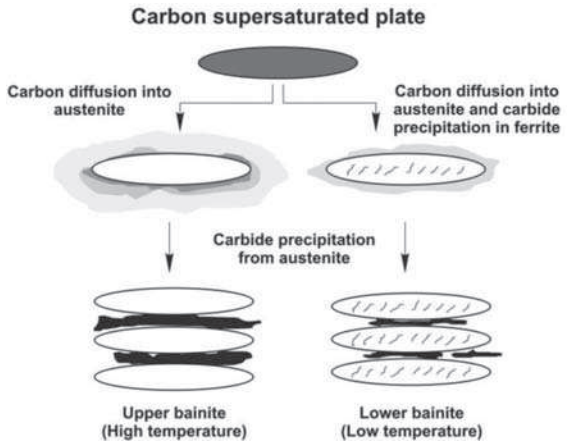

Fig. 1. Explanation of the bainitic morphologies formation by means of displacive mechanism [7]

Rys. 1. Wyjaśnienie formowania morfologii bainitu z udziałem mechanizmu ścinania [7]

Consequently, the appearance of the carbides with respect to bainitic ferrite can be used to distinguish both morphological types of bainite. This early classification of bainite has been supported by varying relation between strength and toughness for both types of bainitic structure. However, it was found that Si, Al or even P strongly retards the precipitation of iron carbides during the bainitic transformation [2]. This causes the enrichment of residual austenite in carbon, and as a consequence, decreases of M_s/M_f to room temperature or below, which maintains retained austenite in the structure. The effect of retained austenite on mechanical properties of bainitic steels has not been recognised until 80's although researches indicated the improvement of strength versus ductility relation due to the presence of this constituent in their structure.

This improvement is significant when the stability of retained austenite against the deformation is high, and this feature mostly depends on its carbon content. The improvement in strength and ductility is explained by the so called transformation induced plasticity (TRIP) effect. Namely, during the deformation, austenite gradually transforms to martensite in the mostly strained region of the material which causes substantial work hardening and prevents against the plastic flow localisation. One of the most distinct feature of bainite is the incomplete transformation phenomenon which is manifested by the suppression of austenite decomposition prior to reaching equilibrium of value for the transformation temperature. Bhadeshia and Edmonds explained this considering that the bainite ferrite formation is a displacive transformation followed by partitioning of carbide into surrounding austenite [7]. As a consequence of this partitioning, new bainite subunits are growing from the more and more carbon saturated austenite. This increases the free energy of ferrite and decreases the free energy of austenite (Fig. 2).

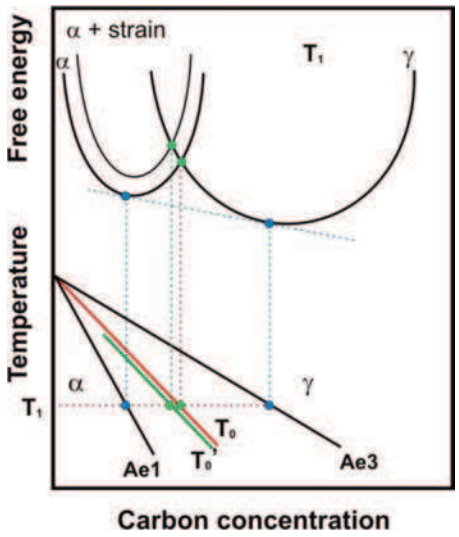

Fig. 2. Definition of the T_0 and T_0' line using the thermodynamic concept [7]

Rys. 2. Definicja linii T_0 i T_0' zgodnie z koncepcją termodynamiczną [7]

At temperature referred to as T_0 both free energies are equal and the growth of bainite subunits is not possible anymore. However, when the stored energy of bainitic ferrite due to the shape changes accompanying transformation is taken into account, the T_0 line shifts into a new position, which conventionally is referred to as T_0' line.

In the Bhadeshia and Edmons's approach to bainitic transformation, the nucleation process is diffusion controlled, however, the growth of bainite subunit is diffussionless. The minimum driving force for nucleation of bainitic and Widmanstattän ferrite can be represented by the following equation:

$$\Delta G_N \left(\frac{\mathrm{J}}{\mathrm{mol}}\right) = 3,637(T - 273,18) - 2540 \qquad (1)$$

The following conditions for bainite formation were defined:

$$\Delta G^{\gamma\to\alpha} < -G_{SB} \qquad (2)$$

$$\Delta G_m < G_N$$

where:

$\Delta G^{\gamma\to\alpha}$ – free energy change connected with difussionless transformation in J/mol;

ΔG_m – free energy change available for nucleation under diffusion in J/mol;

G_{SB} – is the stored energy of bainite (400 J/mol).

The difficulties in maintaining stable bainite morphology in subsequent technological stages are connected with a strong effect of cooling rate and austenite microstructure on the bainitic transformation. Depending on the steel chemical composition, austenite state and cooling conditions, different morphological types of bainite microstructure can be developed (Fig. 3 and 4). The classification of bainite in Fig. 3 was taken after Zając et al. [8]. In continuous cooling conditions, different types of bainite may be obtained which results in nonhomogeneous steels microstructure (Fig. 4).

From Fig. 4, one can see that typically different bainite morphologies can be developed during continuous cooling of a steel. Thus, the only way of obtaining the degenerated upper bainite, which is the most promising microstructure for advanced applications, is through applying the low temperature isothermal treatment, i.e., below 450°C.

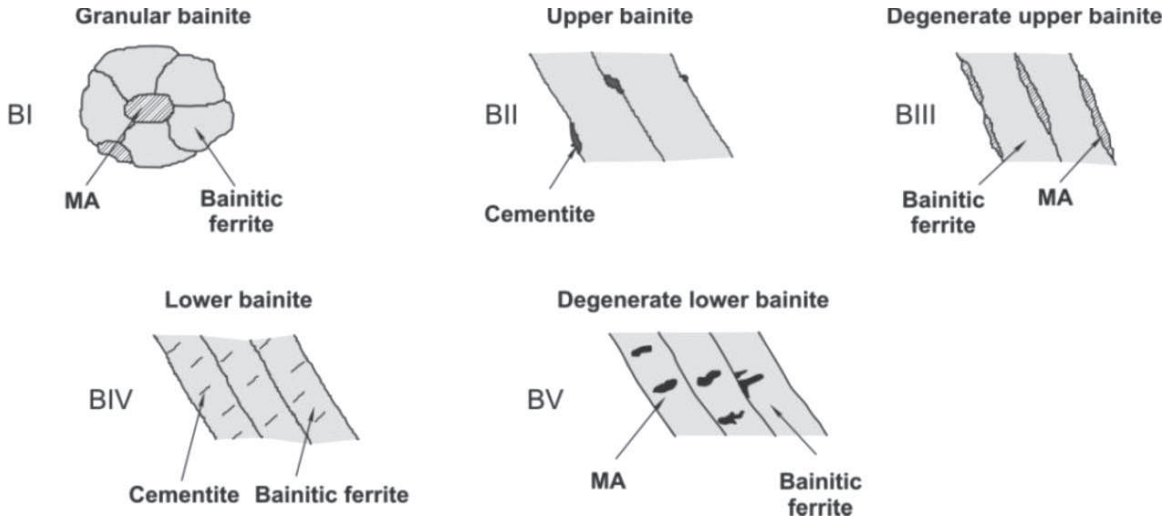

Fig. 3. Classification of different types of bainite microstructure [8]

Rys. 3 Klasyfikacja różnych typów struktury bainitu [8]

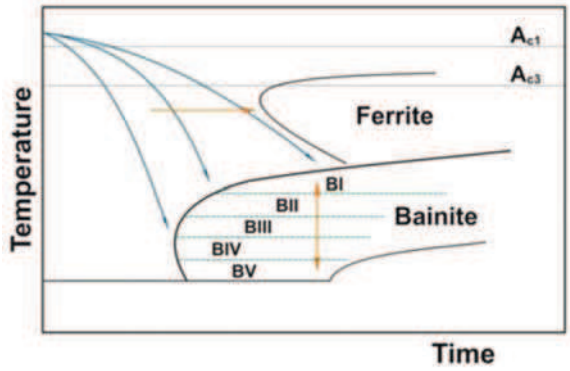

Fig. 4. Effect of cooling conditions on the morphology of bainite

Rys. 4. Wpływ warunków chłodzenia na morfologię bainitu

3. MATERIAL AND EXPERIMENTAL METHODOLOGY

The chemical composition of the experimental steel is given in Table 1. The heat was melted in VSG100 laboratory furnace and cast into 70 kg ingot having cross section 160×160 mm. A piece of this ingot was further forged into rod having 15 mm in diameter. The cylindrical samples were machined from the rod having dimensions Φ 5×7 mm for the phase transformation investigations with deformation dilatometer DIL 805A/D.

Table 1. Chemical composition (in mas.%) of the laboratory heat

Tabela 1. Skład chemiczny wytopów laboratoryjnych (w % masowych)

Heat	C	Si	Mn	S	Cr	Mo	Ni	Cu	Al
S369	0.23	0.98	1.52	0.14	1.51	0.14	0.072	0.01	<0.005

Physical simulation of thermomechanical processing was conducted with Gleeble 3800 simulator. The plane strain multi-deformation experiments were conducted on samples with dimensions: 15 mm × 20 mm × 35 mm. A schematic picture showing the appearance of the as deformed sample and the preparation of the specimens for mechanical properties measurement and microstructure investigation is shown in Fig. 5. The scope of the experiments is presented in the following sections.

Light optical microscopy (LOM), scanning electron microscopy (SEM), electron backscatter diffraction (EBSD) and X-ray diffraction were used to characterize the microstructure of the specimens subject to different thermo-mechanical cycles. One of the main goals of the structure examination was the identification of the retained austenite occurrence and measurement of its volume fraction as well as carbon content in this constituent.

The samples subject to the X-ray analysis were polished and etched with HCL. The analysis was conducted with an Empyrean difractometer using cobalt radiation and Pixel detector.

The experimental conditions were as follows:
- angular range: 48÷104° 2θ;
- measurement step: 0,02626° 2θ;
- counting time: 200 s;
- measured diffraction lines: A: (111), (200), (220) and BF: (110), (200), (211).

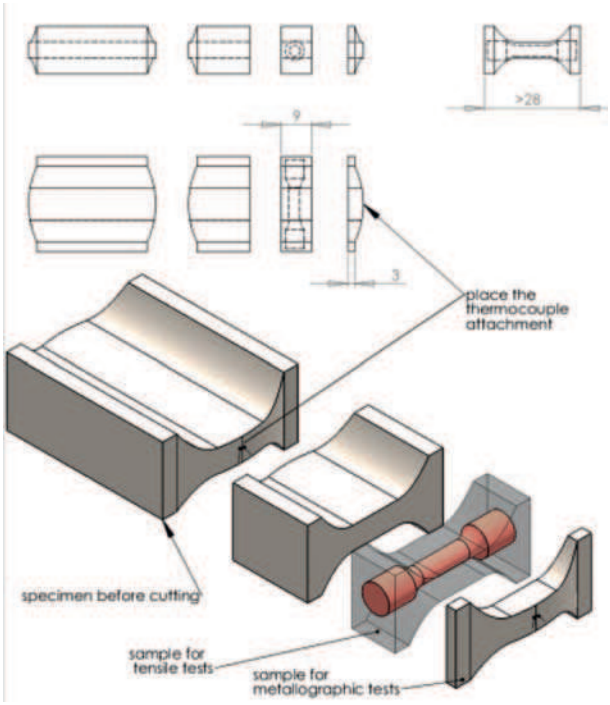

Fig. 5. Sample after the thermo-mechanical processing with Gleeble 3800 system and the specimens preparation for further tests

Rys. 5. Próbka po obróbce termo-mechanicznej na symulatorze Gleeble 3800 i przygotowanie próbek do dalszych badań

The Averbach & Cohen'a metod was applied for the measurement of the retained austenite content [9]:

$$V_A = \frac{1/n_A \sum \frac{I_A^{hkl}}{R_A^{hkl}}}{1/n_M \sum \frac{I_A^{HKL}}{R_A^{HKL}} + 1/n_A \sum \frac{I_A^{hkl}}{R_A^{hkl}} + V_C} \quad (3)$$

where:
- I – integrated intensities of experimental lines,
- n – number of the diffraction line
- R – theoretical intensity, given by the following equation:

$$_R = \frac{1}{v^2} |\bar{F}|^2 pLPe^{-2M} \quad (4)$$

where:
- a – lattice constant
- $V = a^3$
- $LP = f(2\theta, 2\alpha)$
- P – multiplicity factor of atomic planes *(hkl)*
- F – atomic scattering factor = $f_0 + \Delta f$

The High Score Plus program was used to fit the measured reflexes and AS program for the calculation of retained austenite content.

The carbon content in retained austenite, C_γ, was calculated trough lattice parameter measurement, a_γ, and equation [10]:

$$C_\gamma = (a_\gamma - 0.3555)/0.0044 \quad (5)$$

As seen in Fig. 5, non-standard specimens were used in the tensile test which is connected to a small size of the samples subject to deformation in Gleeble 3800 simulator. This affects, most of all, the assessment of the total elongation, however, has no significant effect on the accuracy of strength properties measurement.

4. BALANCING THE CCT DIAGRAM AND TRANSFORMATION KINETICS TO IMPROVE THE MECHANICAL PROPERTIES OF BAINITIC STEELS

4.1. CONTINUOUS COOLING AT CONSTANT COOLING RATES

Majority of rolled steel products is continuously cooled from the austenite state. Therefore, the first insight into the possible microstructural constituents that could be formed at different cooling conditions was obtained by analysing the CCT diagrams. The investigation was carried out after heating the specimens up to temperature 1210°C at heating rate of 3°C/s. The austenitizing time at this temperature was 60 seconds. The deformation (upsetting) of the specimens was performed at two temperatures: 1150°C and 1050°C at strain rate of 1 s^{-1}. The values of logarithmic strain at each temperature were assumed respectively: $\varepsilon_1 = -0.30$ and $\varepsilon_2 = -0.39$. The cooling rate to deformation temperatures was 2°C/s. Before deformation specimens were kept at the deformation temperature for 5 seconds. After the last deformation, the specimens were cooled at a rate of 50°C/s to 850°C, followed by a 5 seconds holding time and a constant (linear) cooling. Applied cooling rates were: 0.03, 0.05, 0.1, 0.25, 0.5, 1.0, 2.0, 5.0, 10.0, 15.0, 20.0, 40.0°C/s, and maximum rate possible when helium was applied as cooling medium. The maximum cooling rate using helium (100% of valve opening) was calculated as a mean cooling rate between 800°C and 500°C. The microstructure of the sample cooled with maximum cooling rate after holding at 850°C is shown in Fig. 6. The measured prior austenite grain size (equivalent diameter) was 32 µm. The CCT diagram developed in the dilatometric tests is shown in Fig. 7.

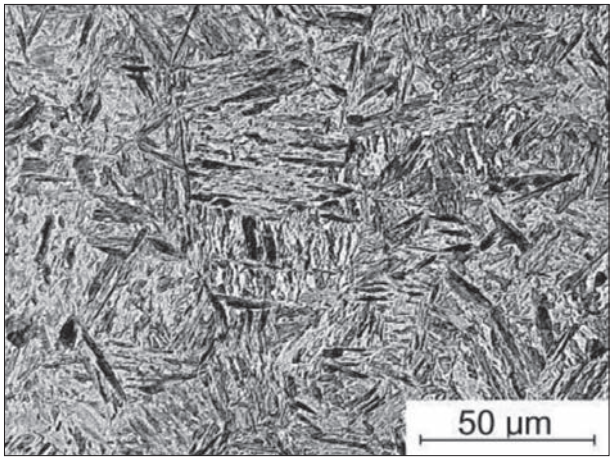

Fig. 6. Microstructure of the dilatometric sample cooled at maximum cooling rate from 850°C; LOM

Rys. 6. Mikrostruktura próbki dylatometrycznej, chłodzonej z maksymalną szybkości chłodzenia od 850°C; LOM

Microstructures of the dilatometric samples for the most relevant cooling conditions to industrial practice are shown in Fig. 8. Results of the analysis of dilatometric curves are presented in Table 2. The results of Table 2 are summarized in Fig. 9.

The data of Table 2 show that the maximum content of retained austenite occurs in the microstructure of the dilatometric samples cooled with the narrow range of cooling rates (0.2÷2.0°C/s) and coincides with the highest values of the bainitic ferrite fraction obtained in the samples. Thus, to be able to stabilise the austenite with carbon, fraction of bainitic ferrite should be at least 30÷50%.

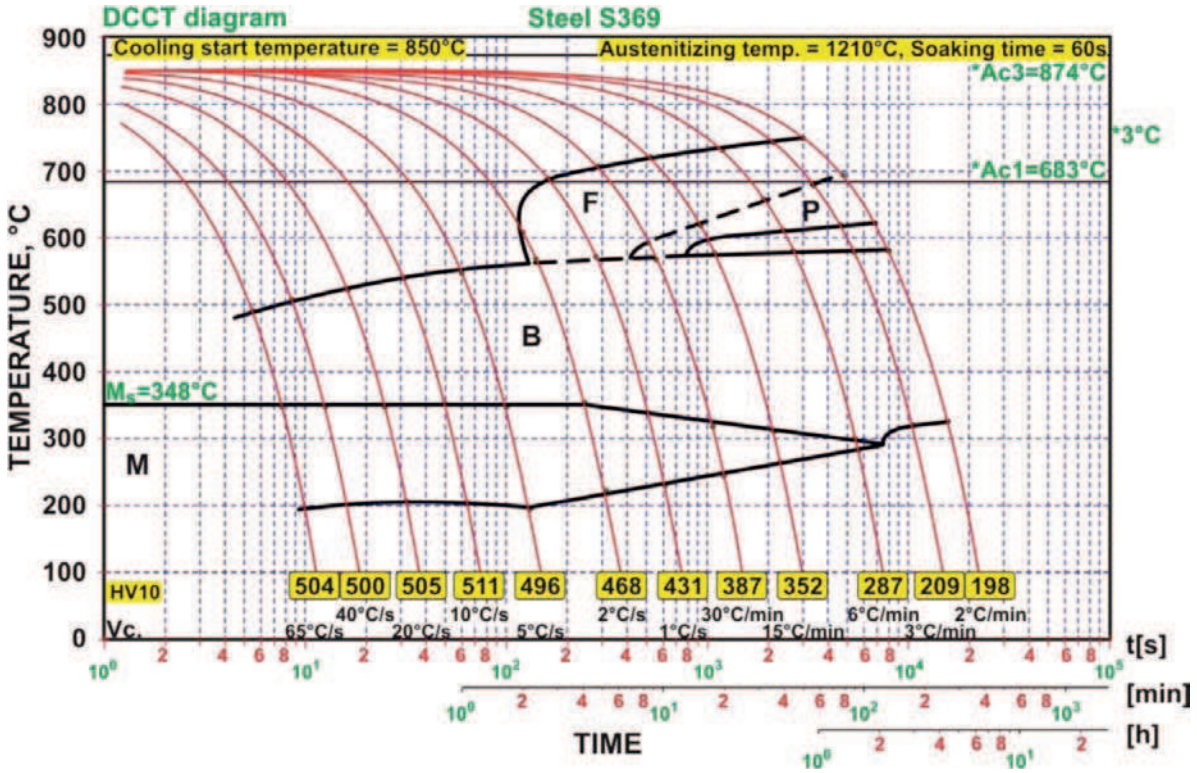

Fig. 7. CCT diagram of experimental steel

Rys. 7. Diagram CCT stali eksperymentalnej

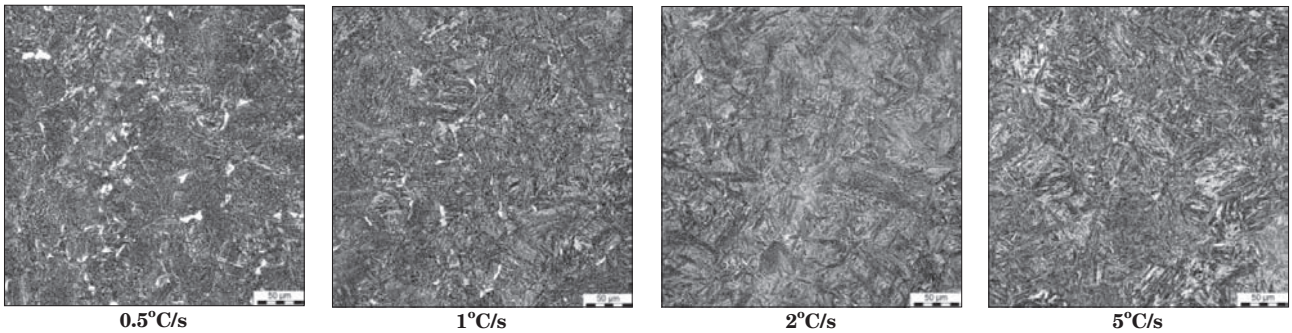

Fig. 8. Microstructures of the dilatometric samples cooled at different rates; LOM

Rys. 8. Mikrostruktury próbek dylatometrycznych chłodzonych z różnymi szybkościami; LOM

Table 2. Volume fraction of the structure constituents of dilatometric samples and carbon content in retained austenite

Tabela 2. Udział objętościowy składników struktury próbek dylatometrycznych i zawartości węgla w austenicie

Volume fraction of phases [in %] in dilatometric samples						
Cooling rate	**F**	**P**	**B**	**M**	**RA**	**C_γ**
2°C/min	34.0	52.0	14.0	0.0	0.0	-
3°C/min	33.0	54.0	13.0	0.0	0.0	-
6°C/min	31.9	16.0	37.0	4.0	11.1	1.21
15°C/min	18.0	6.0	54.0	4.0	18.0	1.25
30°C/min	8.0	4.0	68.0	4.0	16.0	1.11
1°C/s	4.0	0.0	70.0	8.0	18.0	1.25
2°C/s	0.0	0.0	52.0	39.6	8.4	1.21
5°C/s	0.0	0.0	23.0	77.0	0.0	-
10°C/s	0.0	0.0	18.0	82.0	0.0	-
20°C/s	0.0	0.0	10.0	92.0	0.0	-
40°C/s	0.0	0.0	8.0	92.0	0.0	-
84°C/s	0.0	0.0	7.0	93.0	0.0	-

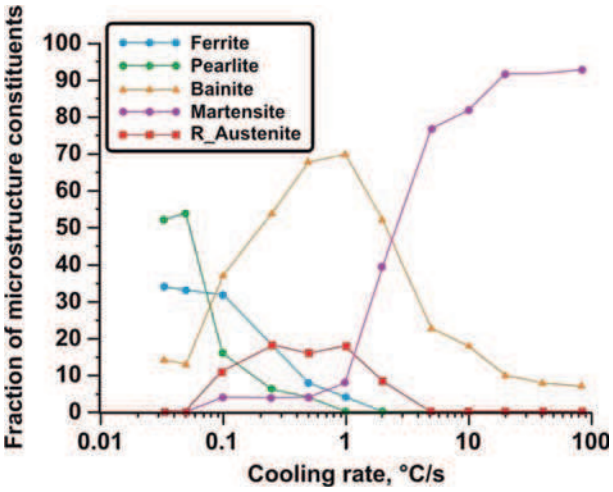

Fig. 9. Effect of cooling rate on the structural constituents fraction in dilatometric samples

Rys. 9. Wpływ szybkości chłodzenia na udział składników strukturalnych w próbkach dylatometrycznych

4.2. ISOTHERMAL HEAT TREATMENTS

The effect of the isothermal treatment on the mechanical properties was investigated by subjecting the samples to the thermal-mechanical processing in Gleeble 3800 simulator. The experiments comprised heating of the sample to 1210°C and holding at this temperature for 60 seconds followed by the sequence of deformations and controlled cooling. The stress – strain curve for the test is given in Fig. 10. The deformation temperatures and time intervals between subsequent deformations are also specified in this figure. The appearance of stress – strain curve shows that the static recrystallization of austenite is almost completed during time intervals between three last deformations. The cooling schedule of the samples after the last deformation comprised fast cooling at rate around 20°C/s to temperatures in the range 375÷500°C followed by holding at these temperatures for 50, 100 and 500 se-

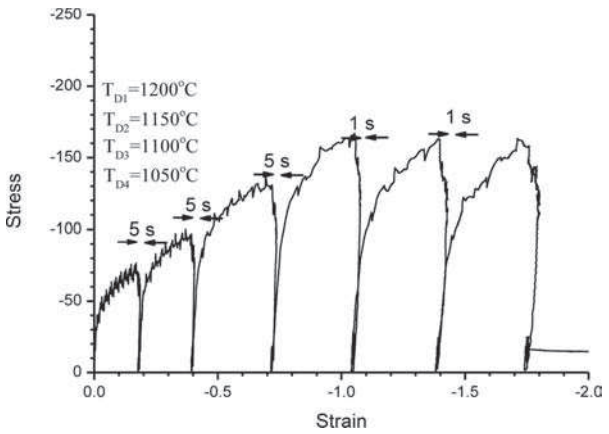

Fig. 10. Stress-strain curves for the multi-deformation experiments conducted in Gleeble 3800; T_{D1}-T_{D4} are temperatures of subsequent deformations

Rys. 10. Krzywe naprężenie-odkształcenie uzyskane w doświadczeniach wielostopniowego odkształcenia w symulatorze Gleeble 3800

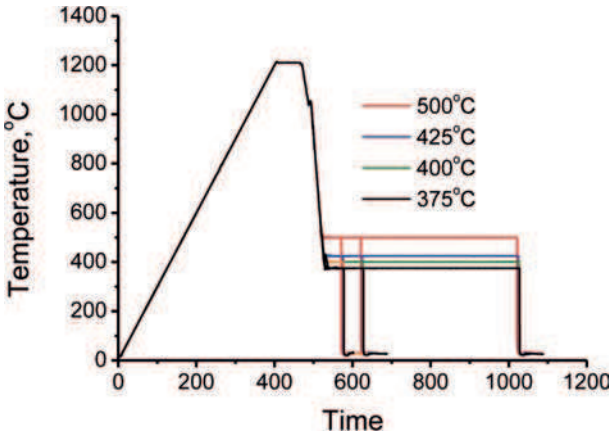

Fig. 11. Temperature versus time changes in the conducted tests

Rys. 11. Zmiany temperatury w funkcji czasu w przeprowadzonych testach

conds. Following holding, the samples were fast cooled with water. The thermal profiles for the conducted tests are shown in Fig. 11.

Microstructures of the samples subject to experiments in Gleeble 3800 system are shown in Fig. 12–15. The mechanical properties of the samples are given in Table 3 and are compared in Fig. 16.

Micrographs in Fig. 12–15 show that the structure of the samples is depended on temperature and time of the isothermal holding. Shorter holding times at subsequent temperatures result in higher martensite content in the samples. This means that austenite was not stable due to the low content of carbon in this phase. At higher transformation temperatures, i.e. above 425°C, the structure of the samples is mostly composed of granular bainite whilst degenerated upper bainite is mostly observed at lower transformation temperatures.

With the exception of holding temperature of 500°C, increasing the holding time at lower temperatures causes the strength increase and simultaneous decrease of ductility of the samples. The observed effect of isothermal holding temperature at 500°C can be explained in terms of the highest martensite content in the samples held at this temperature. At lower temperatures, presumably the formation of fine structure of degenerated upper bainite is crucial for obtaining high strength level of the steel. The measured volume fraction of retained austenite in the samples subject to Gleeble 3800 experiments is given in Table 4. One can see that X-ray examination did not reveal the presence of retained austenite in the samples held at 500°C. The austenite fraction and carbon content at the isothermal holding temperatures calculated using T_0' concept are given in Table 4 for reference.

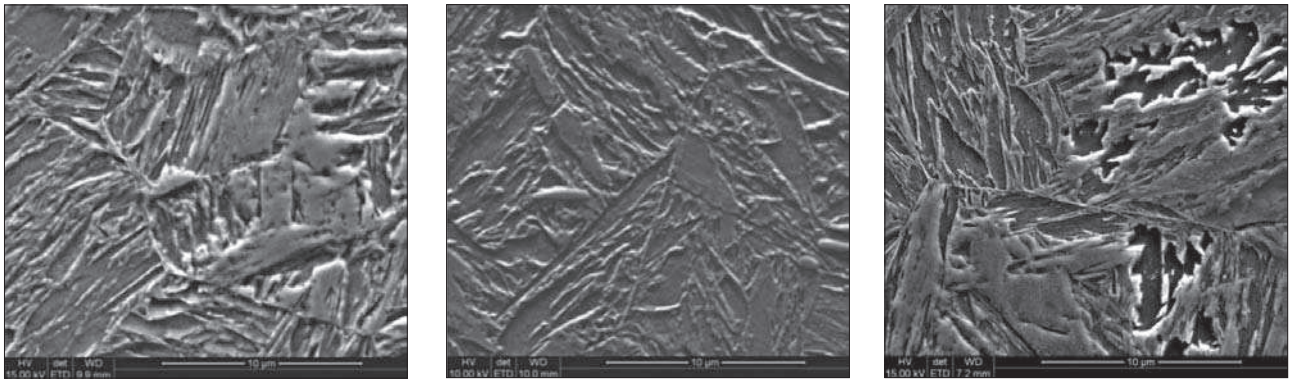

50 s **100 s** **500 s**

Fig. 12. Microstructure of the samples after experiment conducted in Gleeble 3800 simulator with holding temperature 500°C; FEG_SEM

Rys. 12. Mikrostruktura próbek po eksperymentach symulacji fizycznej za pomocą symulatora Gleeble 3800 z temperaturą wytrzymania 500°C; FEG_SEM

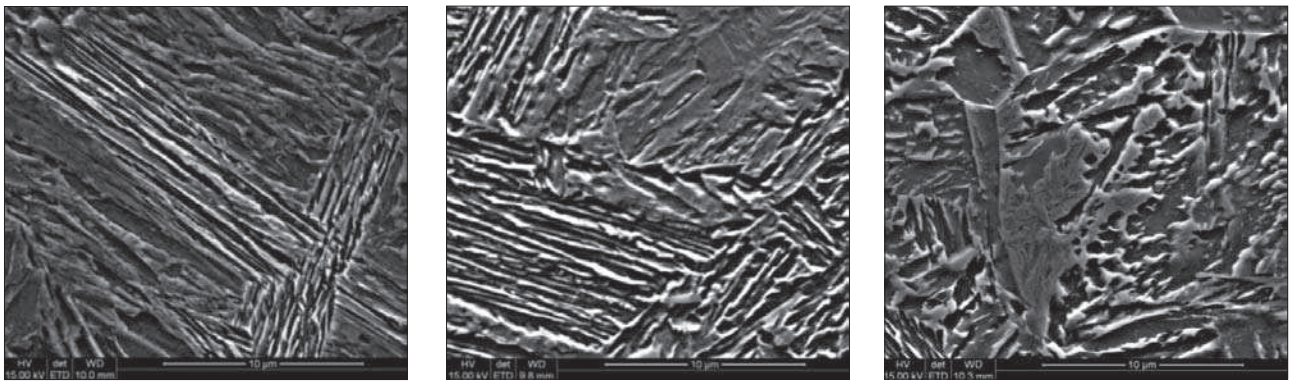

50 s **100 s** **500 s**

Fig. 13. Microstructure of the samples after experiment conducted in Gleeble 3800 simulator with holding temperature 425°C; FEG_SEM

Rys. 13. Mikrostruktura próbek po eksperymentach symulacji fizycznej za pomocą symulatora Gleeble 3800 z temperaturą wytrzymania 425°C; FEG_SEM

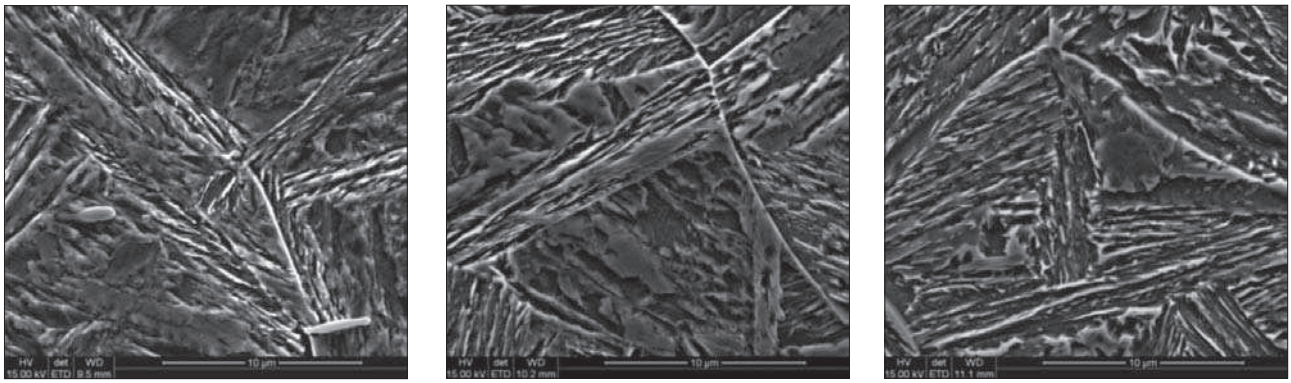

50 s **100 s** **500 s**

Fig. 14. Microstructure of the samples after experiment conducted in Gleeble 3800 simulator with holding temperature 400°C; FEG_SEM

Rys. 14. Mikrostruktura próbek po eksperymentach symulacji fizycznej za pomocą symulatora Gleeble 3800 z temperaturą wytrzymania 400°C; FEG_SEM

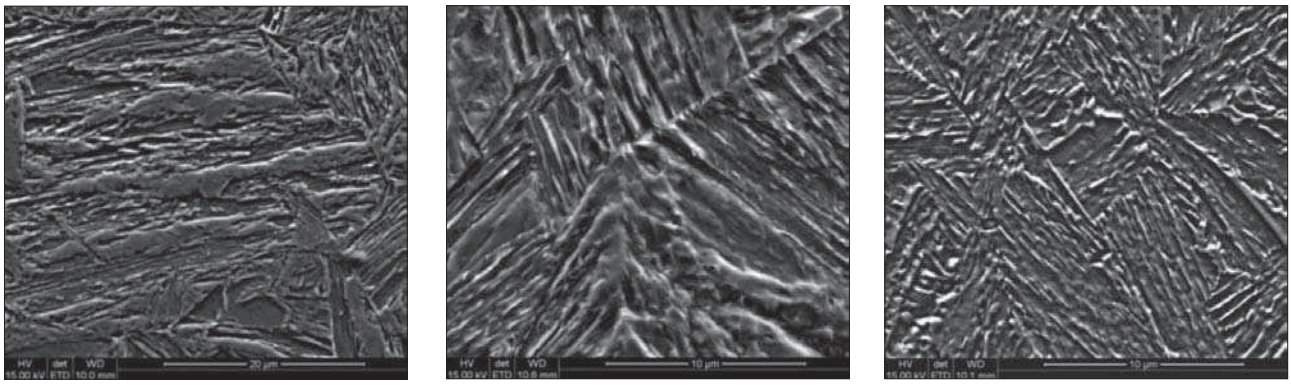

50 s **100 s** **500 s**

Fig. 15. Microstructure of the samples after experiment conducted in Gleeble 3800 simulator with holding temperature 375°C; FEG_SEM

Rys. 15. Mikrostruktura próbek eksperymentach po symulacji fizycznej za pomocą symulatora Gleeble 3800 z temperaturą wytrzymania 375°C; FEG_SEM

Table 3. Mechanical properties of the samples subject to Gleeble experiments

Tabela 3. Właściwości mechaniczne próbek po eksperymentach symulacji fizycznej za pomocą symulatora Gleeble

Sample ID	Temp | time	$R_{p0.2}$	R_m	Z	A
		MPa	MPa	%	%
HP141111.D02	500°C/500 s	1046	1532	11.1	8.5
HP141112.D01	500°C/100 s	1028	1469	12.3	7.8
HP141113.D01	500°C/50 s	1354	1677	17.4	9.7
HP141114.D01	425°C/500 s	822	1300	16.6	16.1
HP141115.D01	425°C/100 s	968	1387	11.7	10
HP141116.D01	425°C/50 s	1248	1652	6.6	8.6
HP141117.D01	400°C/500 s	988	1317	12.9	15.2
HP141118.D01	400°C/100 s	1020	1455	14.9	10.2
HP141119.D01	400°C/50 s	1282	1685	11.1	8.7
HP141120.D02	375°C/500 s	1060	1410	17.9	11.1
HP141121.D01	375°C/100 s	1117	1515	12.3	7.2
HP141122.D01	375°C/50 s	1326	1651	12.3	7.5

The most important aim of the chemical composition and processing parameters design of TRIP assisted bainitic steels is to obtain a proper balance between strength and ductility of the product. Thus, to select the optimal isothermal heat treatment conditions, a plot of $R_m(A/100)$ product for samples subject to Gleeble experiments is shown in Fig. 17.

The results indicate that the best combination of strength and ductility is related to the volume fraction of retained austenite, but also morphology of this phase is important. The maximum value of $R_m(A/100)$ product is observed in samples having maximum volume fraction of degenerated bainite in which the retained

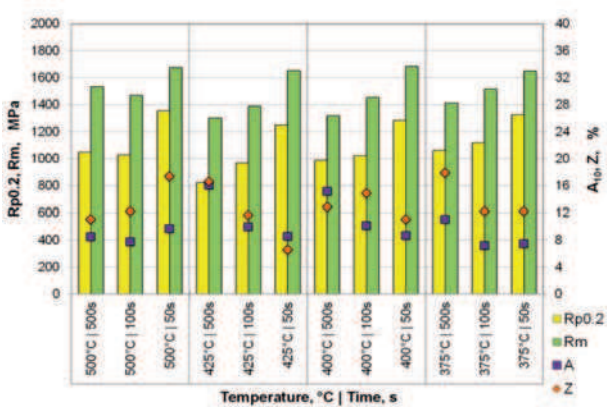

Fig. 16. Summary of the results of mechanical properties measurements for the samples after experiments conducted in Gleeble 3800 thermomechanical simulator

Rys. 16. Podsumowanie wyników pomiaru właściwości mechanicznych próbek po eksperymentach symulacji fizycznej za pomocą symulatora Gleeble

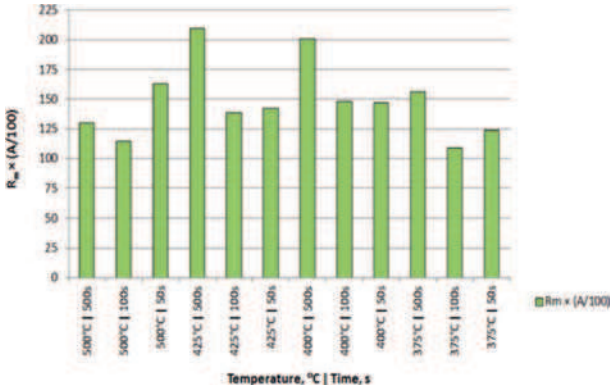

Fig. 17. Effect of isothermal holding temperature and time on $R_m(A/100)$ product for the samples subject to physical simulation experiments conducted with Gleeble 3800

Rys. 17. Wpływ temperatury i czasu izotermicznego wyżarzania na parametr $R_m(A/100)$ dla próbek po eksperymentach symulacji fizycznej za pomocą symulatora Gleeble 3800

Table 4. Measured volume fraction of the retained austenite in the samples subject to experiments in Gleeble 3800 simulator

Tabela 4. Wyznaczony udział objętościowy austenitu szczątkowego dla próbek po eksperymentach symulacji fizycznej za pomocą symulatora Gleeble

Sample specification	Temp | Time	Retained austenite	Carbon content in austenite	Calculated carbon content	
	°C | s	% vol.	%	T_0, %	T_0', %
HP141111.D02	500 | 500	no X-ray lines detected	-	-	-
HP141112.D01	500 | 100	no X-ray lines detected	-	-	-
HP141113.D01	500 | 50	no X-ray lines detected	-	-	-
HP141114.D01	425 | 500	18.8	1.11	1.02	0.95
HP141115.D01	425 | 100	15.6	1.19		
HP141116.D01	425 | 50	1.8	1.14		
HP141117.D01	400 | 500	12.0	1.10	1.06	1.02
HP141118.D01	400 | 100	12.6	1.16		
HP141119.D01	400 | 50	2.3	1.16		
HP141120.D02	375 | 500	13.7	1.08	1.08	1.13
HP141121.D01	375 | 100	11.7	1.19		
HP141122.D01	375 | 50	1.6	1.09		

austenite is mostly in the form of thin layers located between laths of bainitic ferrite (Fig. 18 and 19).

The obtained results show that the formation of retained austenite is connected with crystallographic lattice imperfections. At higher transformation temperatures, where granular bainite forms, it mostly nucleates at dislocation substructure. On the contrary, at lower temperatures where degenerated upper bainite forms, it is mostly connected with bainitic ferrite laths boundaries.

5. EXPERIMENTS OF RODS COOLING FROM TEMPERATURE OF AUSTENITE STABILITY

The CCT diagram in Fig. 7 was developed under constant cooling rate which is maintained during the experiment by the steering system of the dilatometer. However, in real industrial conditions the transformation heat (recalescence effect) can affect the kinetics of phase transformations. The experiments of rods cooling were performed to investigate the interaction of different cooling conditions and released heat of bainitic transformation on the microstructure and mechanical properties of experimental steel. The rods having diameters 6.5, 12, 18, 25 and 35 mm and 200 mm in height were austenitized at 1050°C for 600 seconds and afterwards cooled in still air. The temperature changes were recorded by thermocouples inserted in drilled holes in the centre of the rods, and the results of the measurements are shown in figure 20.

The temperatures B_s and M_s drawn with a dotted line in Fig. 20 were calculated with JMatPro program. Fig. 20 shows that bainitic transformation generates a significant recalescence effect in the cooling curves. This means that this transformation proceeds in nearly isothermal conditions. Since decreasing the rod diameter causes the increase in cooling rate, the starting temperature of this effect decreases as the rod diameter decreases. For the rod with lowest diameter, the recalescence effect is weak and is close to the M_s temperature. Microstructures in the rods centre and subsurface area are shown in Fig. 21.

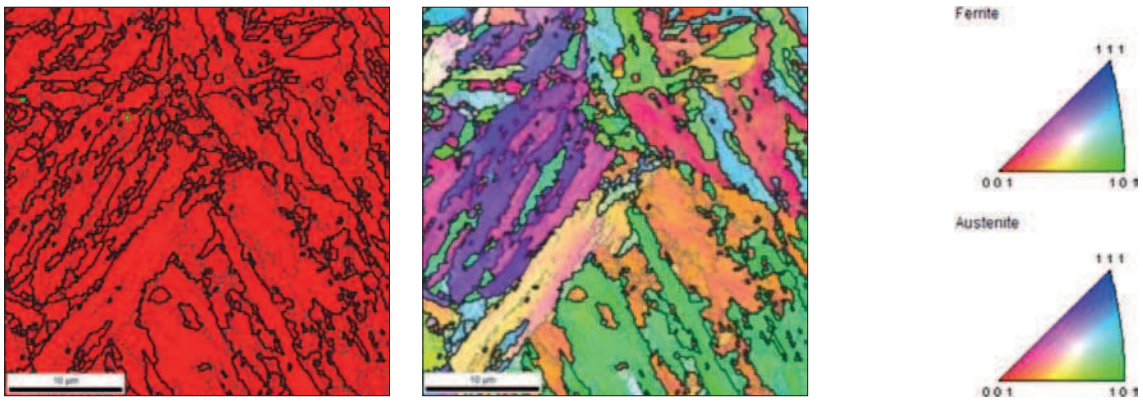

After holding at 500°C for 500 seconds / Po wytrzymaniu w temperaturze 500°C przez 500 sekund

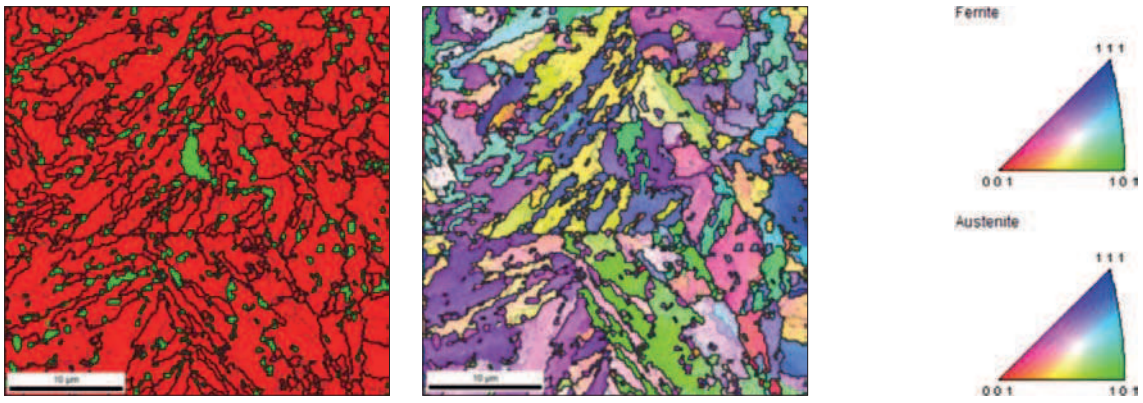

After holding at 425°C for 500 seconds / Po wytrzymaniu w temperaturze 425°C przez 500 sekund

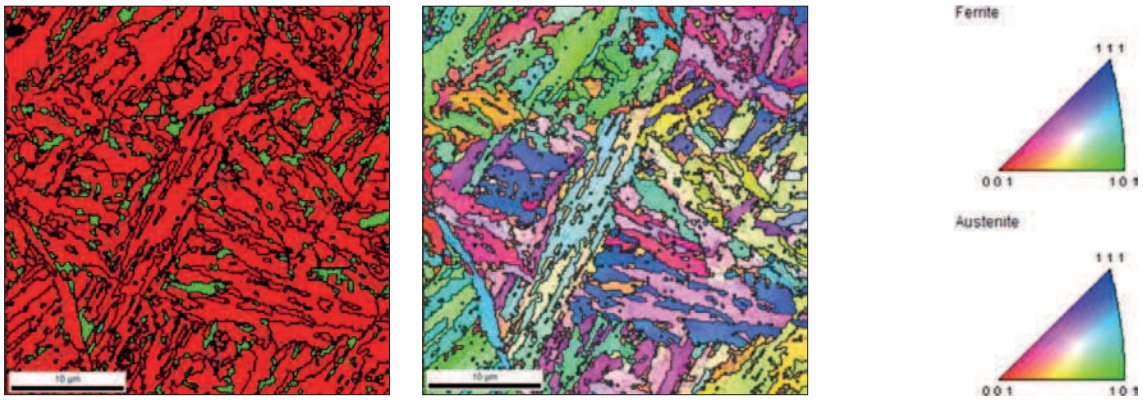

After holding at 400°C for 500 seconds / Po wytrzymaniu w temperaturze 400°C przez 500 sekund

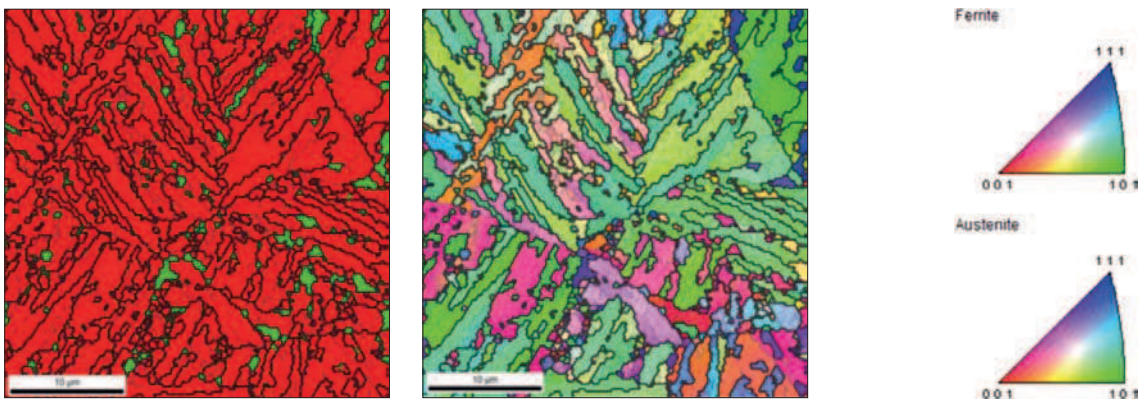

After holding at 375°C for 500 seconds / Po wytrzymaniu w temperaturze 375°C przez 500 sekund

Fig. 18. Phase maps (left hand side) and orientation distribution maps (right hand side) – in dilatometric samples subject to isothermal annealing for 500 seconds; green areas in phase maps stand for retained austenite

Rys. 18. Mapy rozkładu faz (lewa strona) i mapy rozkładu orientacji (prawa strona) – w próbkach dylatometrycznych poddanych wytrzymaniu izotermicznemu przez 500 sekund; obszary zaznaczone kolorem zielonym oznaczają austenit resztkowy

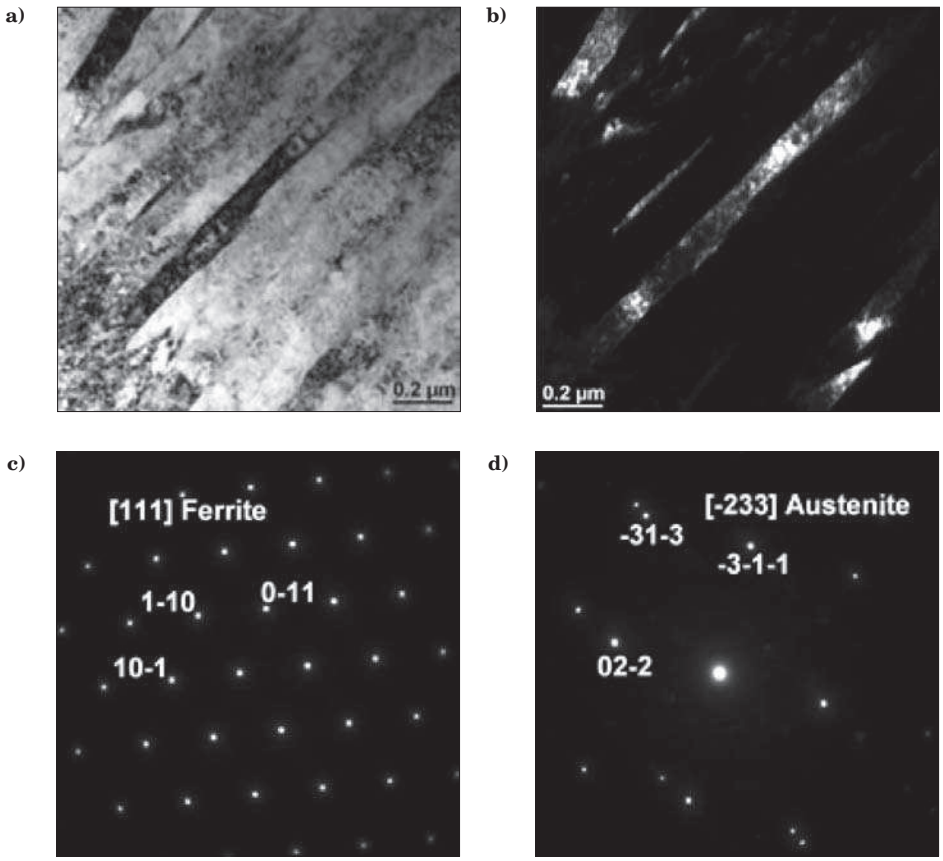

Fig. 19. Microstructure of the sample HP141120 investigated with TEM: (a) micrograph in bright field; (b) dark field electron micrograph with thin films of retained austenite; (c) and (d) diffraction patterns of ferrite and austenite, respectively

Rys. 19. Mikrostruktura próbki HP141120 po badaniach TEM: (a) obserwacje w polu jasnym; (b) ciemne pole z widocznymi cienkimi warstwami austenitu szczątkowego; (c) i (d) obraz dyfrakcyjny odpowiednio dla ferrytu i austenitu

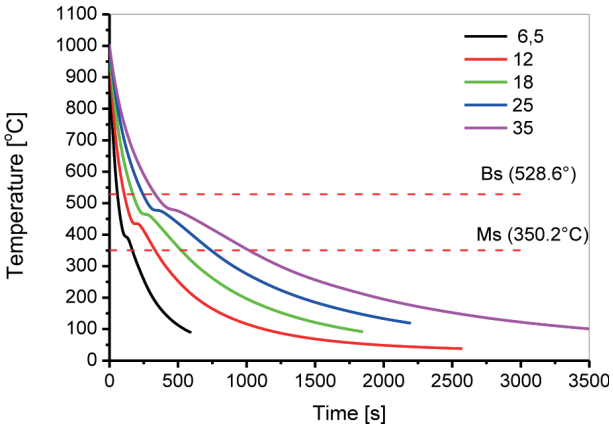

Fig. 20. Temperature changes recorded during cooling by the thermocouples inserted in the drilled hole of the rods having different diameter

Rys. 20. Zmiany temperatury zarejestrowane podczas chłodzenia przez termopary umieszczone w wywierconych otworach w prętach o różnej średnicy

Microstructure of the rod having the smallest diameter (Ø 6 mm) is composed of degenerated upper bainite and blocks of martensite. As the rod diameter increases, the martensite content decreases in the structure and the allotriomorphic and bainitic ferrite content increases. Degenerated upper bainite is mostly observed in rods having diameter in the range 12÷18 mm and in rods having diameter in the range 25÷35 mm, the mixture of granular and degenerated upper bainite is observed.

The mechanical properties of the rods are given in Table 5 and summarized in Fig. 22. The best combination of strength and ductility was obtained for rod having diameter 18 mm which is demonstrated in Fig. 23.

X-ray analysis shows that austenite content is the highest for the rod with diameter 18 mm (Table 6). Therefore some correlation can be found between the austenite content in rods and product R_mA. However, this product is still high for the rod with lowest diameter. This can be explained in terms of the carbon content in retained austenite which is the highest out of all investigated rods and the morphology of this phase which is distributed in the microstructure in form of thin films. Another microstructural parameter that may have an impact on the behaviour of the rods is the so called "effective grain size" of bainitic ferrite. This aspect of the rods' microstructure together with the distribution of austenite in their structure was investigated with EBSD technique (Fig. 24).

Figure 24 shows that decreasing the bainitic transformation temperature through lowering the rod's radius changes the dominant morphology of bainite from granular to degenerated one. The boundaries in the lath like bainitic ferrite are of high angle. And the laths widths are in the range from 1÷4 µm. On the contrary, bainitic areas in the granular bainite are sub-divided into irregular grains separated with high angle boundaries with sizes in the range 5÷25 µm.

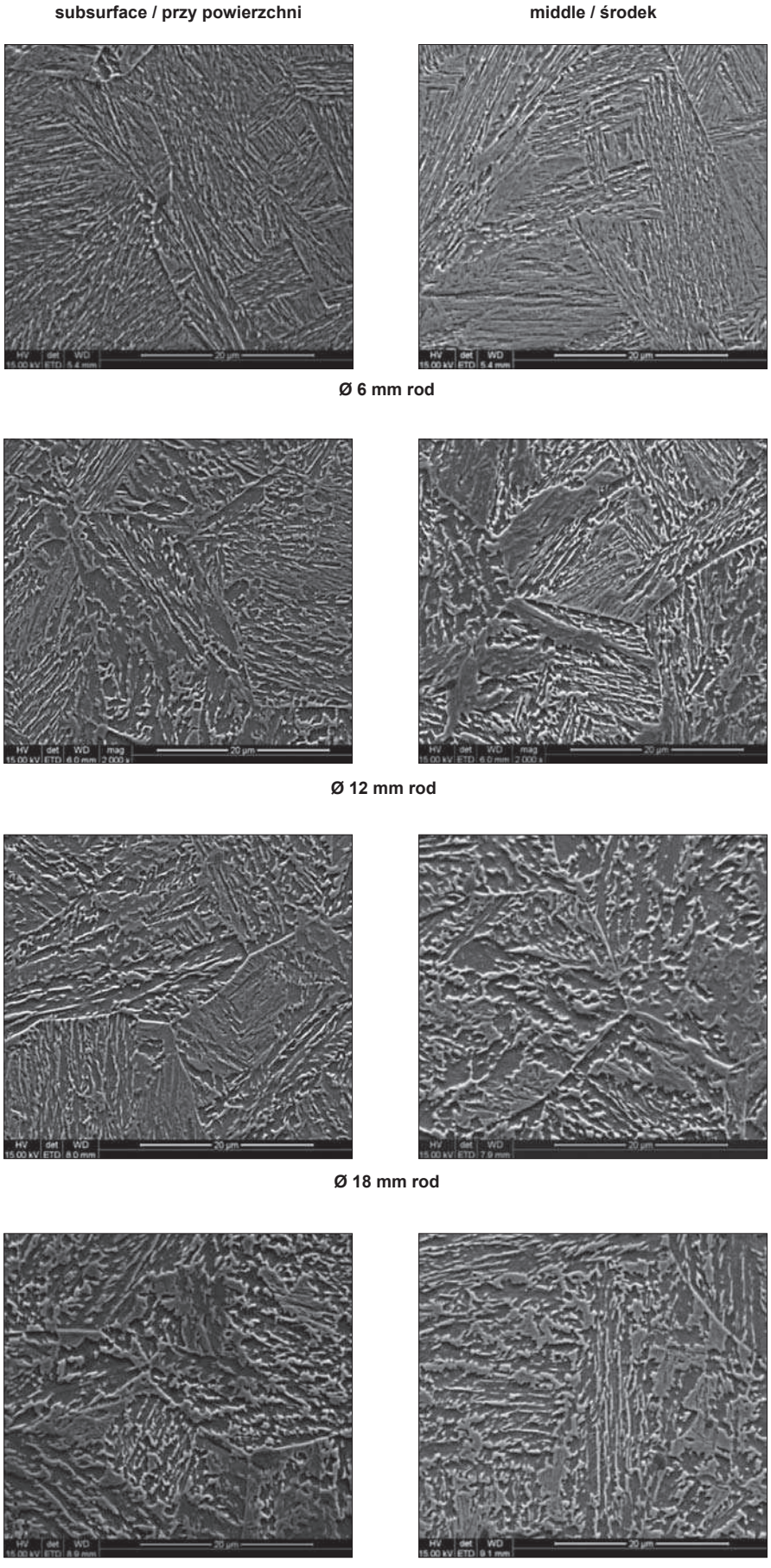

Fig. 21. Microstructure of the rods and subsurface area having different diameter; FEG_SEM; magnification 2000×
Rys. 21. Mikrostruktura prętów o różnej średnicy, FEG_SEM; powiększenie 2000×

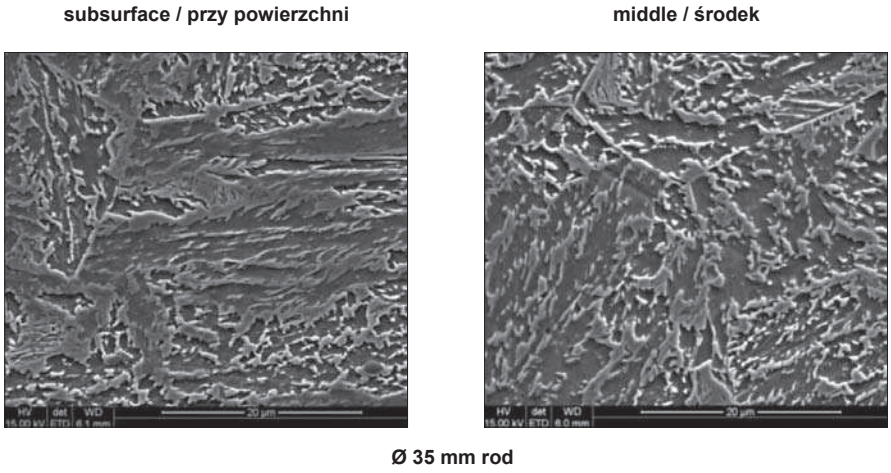

Fig. 21 cont. Microstructure of the rods and subsurface area having different diameter; FEG_SEM; magnification 2000×
Rys. 21 cd. Mikrostruktura prętów o różnej średnicy, FEG_SEM; powiększenie 2000×

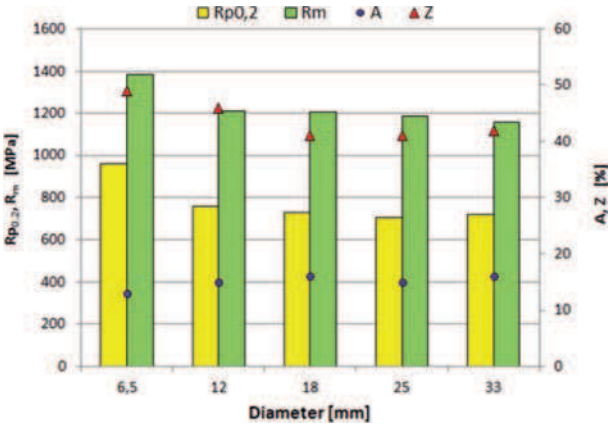

Fig. 22. Mechanical properties of rods with different diameter after cooling in steel air from 1050°C
Rys. 22. Właściwości mechaniczne prętów o różnej średnicy po ochłodzeniu w powietrzu z 1050°C

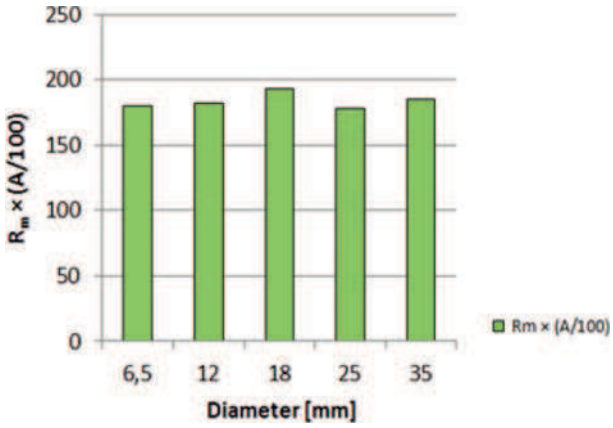

Fig. 23. Product $R_m(A/100)$ for rods with different diameter after cooling in steel air from 1050°C
Rys. 23. Parametr $R_m(A/100)$ dla prętów z różnymi średnicami po chłodzeniu z powietrzu z 1050°C

Table 5. Mechanical properties of the rods after cooling experiments
Tabela 5. Właściwości mechaniczne prętów po eksperymentach chłodzenia

Diameter mm	$R_{p0.2}$ MPa	R_m MPa	A %	Z %
6,5	959	1386	13	49
12	758	1211	15	46
18	728	1207	16	41
25	705	1188	15	41
35	716	1159	16	42

Table 6. Measured volume fraction of the retained austenite in the samples subject to experiments in rods with different diameter
Tabela 6. Wyznaczony udział objętościowy austenitu resztkowego w próbkach prętów o różnych średnicach

Diameter mm	Retained austenite % vol.	Carbon content in austenite%
6.5	10.32	1.40
12	17.68	1.11
18	20.17	1.12
25	16.12	1.08
35	16.03	1.10

Table 7. Recalescence start temperature and cooling rates calculated from cooling curves in Fig. 20
Tabela 7. Temperatura i szybkość chłodzenia wyznaczona na podstawie krzywych chłodzenia z rys. 20

Rod's diameter, mm	T_r °C	Cooling rate °C/s
6	398	2.3
12	437	1.5
18	470	0.9
25	480	0.6
35	484	0.4

To find correlation between the microstructure of the rods and dilatrometric samples, cooling rates in the range $B_s - T_r$, where T_r is a temperature at which the recalescence effect starts, were calculated and are presented in Table 7.

The results of measurement of retained austenite content in rods and dilatometric samples cooled at similar cooling rates are comparable, and as a result the recalescence heat did not affected the phase transformations in the experimental steel significantly. This can be attributed to relatively fast kinetics of bainitic transformation in experimental steel.

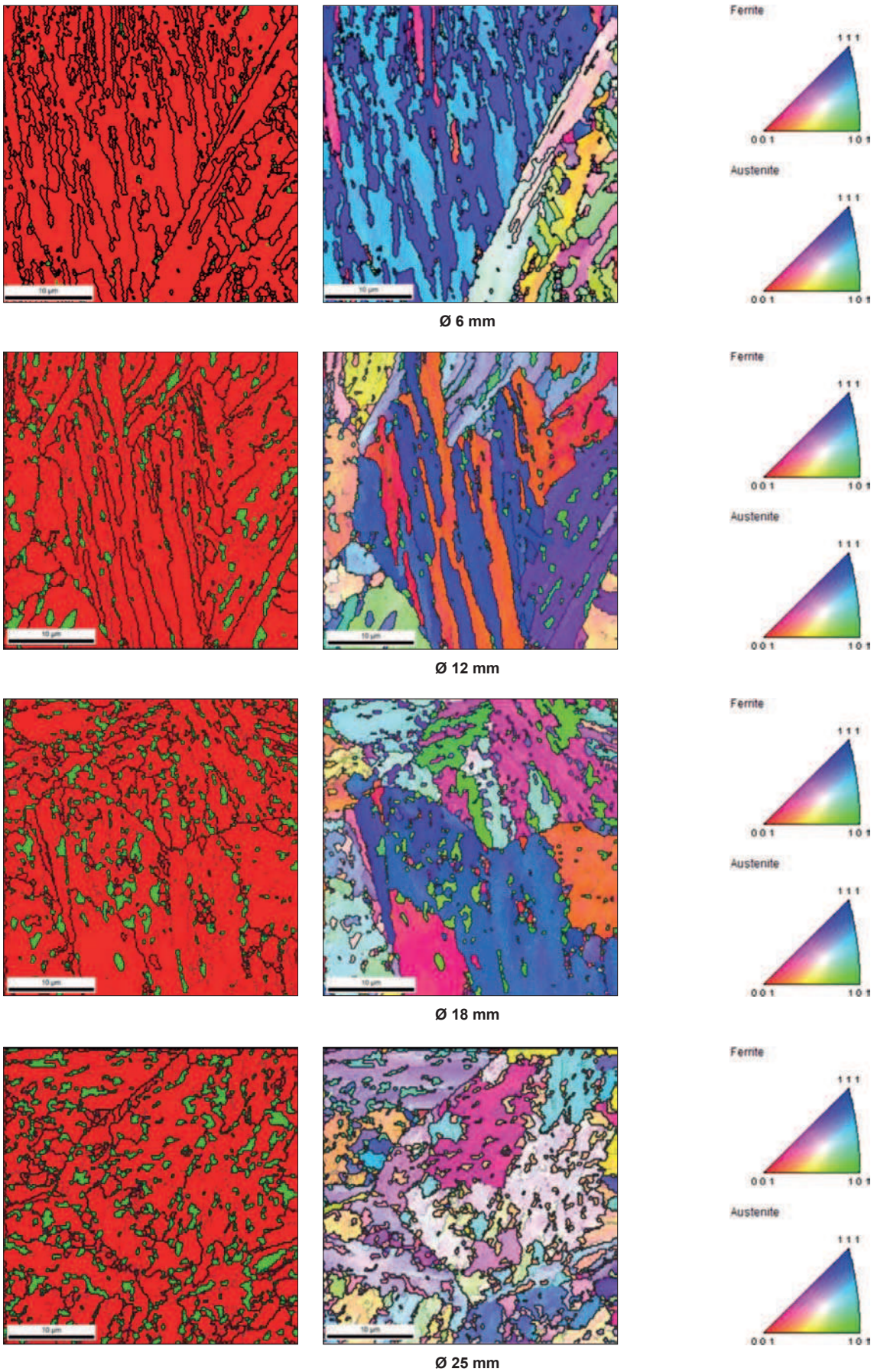

Fig. 24. Phase maps (left hand side) and orientation distribution maps (right hand side) – in the rods' samples subject to continuous cooling; green areas in phase maps stand for retained austenite

Rys. 24. Mapy rozkładu faz (lewa strona) i mapy rozkładu orientacji (prawa strona) – w próbkach poddanych ciągłemu chłodzeniu prętów; obszary zaznaczone kolorem zielonym oznaczają austenit resztkowy

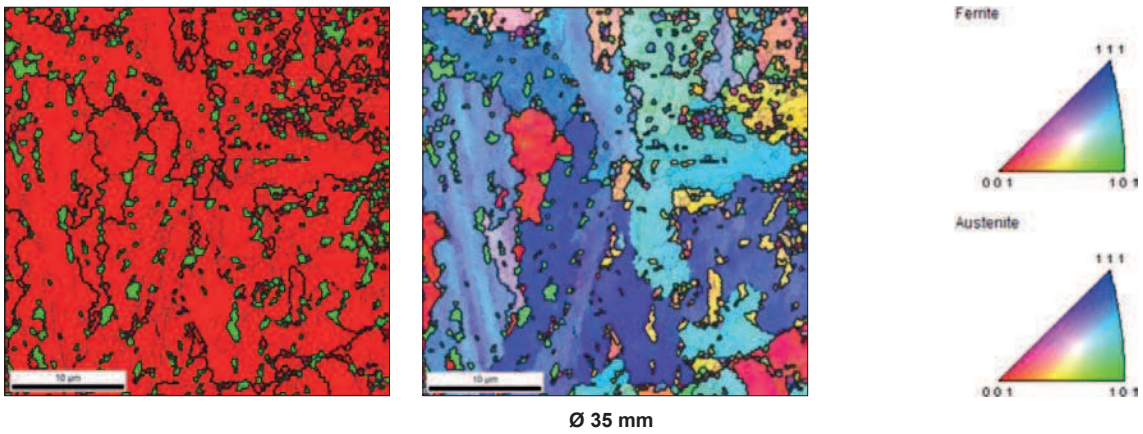

Fig. 24 cont. Phase maps (left hand side) and orientation distribution maps (right hand side) – in the rods' samples subject to continuous cooling; green areas in phase maps stand for retained austenite

Rys. 24 cd. Mapy rozkładu faz (lewa strona) i mapy rozkładu orientacji (prawa strona) – w próbkach poddanych ciągłemu chłodzeniu prętów; obszary zaznaczone kolorem zielonym oznaczają austenit resztkowy

6. APPLICATION OF BAINITIC HARDENABILITY CONCEPT TO OPTIMIZE TRIP EFFECT IN THE BARS

In order to enable comparison of the hardenability of various steels, primary search for certain general indexes, which characterize this hardenability, was made [11]. Evaluation of the capability of various steels to develop bainitic microstructure showed that it is connected with the character of the relation $F_b = F_b(C_r)$, where: F_b – volume fraction of bainite, C_r – cooling rate. This relation is shown for experimental steel in figure 11. The volume fractions of the microstructural constituents can be predicted with *JAMK* equation. Thus, beyond the standard analysis of the CCT diagrams, the following features based on the plot $F_b = F_b(C_r)$, can be considered:

- the area under the curve – the largest is this area the better is the hardenability of steel;
- maximum volume fraction of bainite and the cooling rate, at which this maximum occurs – the larger this maximum is and at lower cooling rate it occurs, the better is the hardenability.

Thus, having the mentioned features in mind the following two hardenability indexes can be considered:

- Ψ_1 – ratio between maximum volume fraction of bainite $V_{b\max}$ and the cooling rate $C_{r\max}$, at which this volume fraction was obtained:

$$\Psi_1 = \frac{V_{b\max}}{C_{r\max}} \tag{6}$$

- Ψ_2 – means the area under the plot $V_b = V_b(C_r)$ in the range, in which volume fraction of bainite exceeds certain level V_{b0};

$$\Psi_2 = \frac{1}{C_{r\max}} \int_{C_{rL}}^{C_{rU}} V_b dC_r \tag{7}$$

Idea of the first hardenability index Ψ_1 is presented in Fig. 25a. The second hardenability index Ψ_2 assuming $F_{b0} = 0.3$ is illustrated in Fig. 25b.

It should be pointed out that the shape of the curve representing bainite content depends not only on the chemistry of steel, but also on the austenite microstructure prior to the beginning of phase transformations.

For the rod production process, only the bainitic hardenability concept based on the relation between volume fraction of bainite and cooling rate was considered in this paper. In order to demonstrate the approach, the commercial Swiss Steel bar having diameter 43 mm was considered. Chemical composition of the bar was: 0.16%C, 1.23% Si, 1.49%Mn, 0.015%S, 1.20% Cr, 0.27%Mo. A comparison of the volume fraction of bainitic ferrite changes as function of cooling rate for this bar and experimental steel is shown in Fig. 26.

Figure 25 shows that reaching the maximum volume fraction of bainitic ferrite in case of industrial bar re-

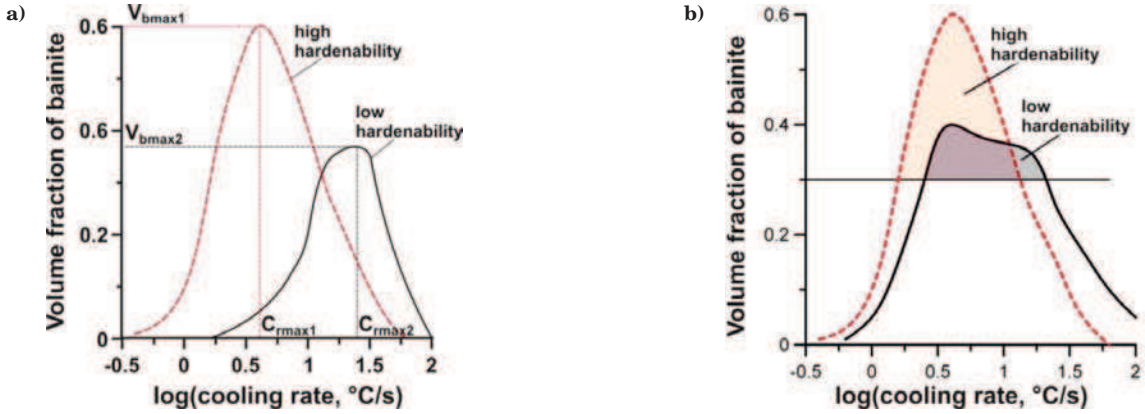

Fig. 25. Idea of the hardenability indexes: definition of Ψ_1 (a); definition of Ψ_2 [10]

Fig. 25. Koncepcja wskaźników hartowności: definicja Ψ_1 (a); definicja Ψ_2 [11]

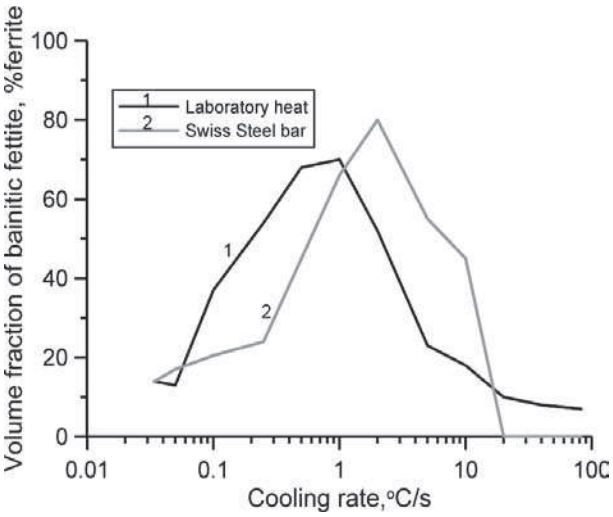

Fig. 26. Comparison of the volume fraction of bainitic ferrite changes as function of cooling rate for laboratory and industrial material assessed in the course of dilatometric experiments

Fig. 26. Porównanie zmian udziału objętościowego ferrytu bainitycznego w funkcji szybkości chłodzenia dla materiału laboratoryjnego i przemysłowego, wyznaczonego po eksperymentach dylatometrycznych

quires higher cooling rates than in the case of laboratory heat, however, the maximum content of this constituent is the highest. A consequence of this is a low bainite content in the industrial bar (cooling rate approximately 0.3°C/s) and, consequently, low retained austenite content (around 10%).

7. CONCLUSIONS

- The transformation of at least 30÷50% of austenite into bainite, is a prerequisite for the retained austenite occurrence in the microstructure of experimental steel. This is connected with the maximum degree of carbon enrichment of austenite remaining after bainitic ferrite formation which is governed by the T_0 or T_0' line.
- The obtained results show that the formation of retained austenite is connected with crystallographic lattice imperfections. At higher transformation temperatures, where granular bainite forms, it mostly nucleates at dislocation substructure. On the contrary, at lower temperatures where degenerated upper bainite forms, it is mostly connected with bainitic ferrite laths boundaries.
- Based upon the obtained results, one may postulate that the formation of retained austenite can be referred to as phase transformation event comprising nucleation and growth. At higher temperatures, where granular bainite forms, it takes random form since the nucleation occurs at the dislocation substructure. However, at low temperatures, it is coordinated with the bainitic laths growth. In both cases, carbon diffusion is the controlling process of retained austenite formation. Thus, the critical carbon content must be reached at nucleation site to start the process of this constituent formation.
- The occurrence of blocky martensite is connected with too low carbon content in the austenite region where it was formed.
- Investigation has shown that the degenerated upper bainite with retained austenite films separating bainitic ferrite laths is the best microstructure for achieving the favourable combination of high strength and ductility. In the experimental steel, this type of bainite can be obtained during isothermal holding at temperature range 430÷370°C. It was observed that at higher isothermal holding temperatures, mostly granular bainite was formed in the samples.
- Since the bainitic transformation temperature range in the continuously cooled rods is higher than 450°C, the main form of bainite in their structure was granular bainite.
- The recalescence effect connected with bainitic transformation has a positive effect on microstructure of the rods, since it extends the time for the bainite formation during continuous cooling.
- The obtained results indicate that not only retained austenite content and morphology have positive effect on strength versus ductility relation, but also the bainitic ferrite effective grain size may have a substantial effect on this relation. At low transformation temperatures, the bainitic ferrite is arranged in form of laths separated by high angle boundaries. In the case of granular bainite, the bainitic ferrite is in the form of irregular grains having size several times greater compared to the laths width.
- The bainitic hardenability concept based on the relation between volume fraction of bainitic ferrite and cooling rate obtained as a result of dilatometric experiments turned out to be a promising tool in the process of designing of the chemical composition of TRIP-assisted bainitic steels.

LITERATURE

1. Bhadeshia H.K.D.H.: Bainite in steels, The Inst. Of Mater., London, 1991
2. Timokhina I.B., Hodgson P.D., Pereloma E.V.: Metall. Mat. Trans. A, vol. 35A, 2004, 2331
3. Jimenez-Melero E., van Dijak N.H., Zhao L., Sietsma J., Offerman S.E., Wright J.P., van der Zwaag S.: Acta Mat., vol. 57 (2009), 533.
4. Habraken L.J., Economopoulos M.: Bainitic structures in low-carbon alloy steels and their mechanical properties, Transformation and Hardenability in Steels, Climax Molybdenium, 1967, 69-108
5. Z. Bojarski, T. Bołd; Acta Metall., Vol. 22 (1974), 1223
6. Ohmori Y., Ohtani H., Kunitake T.: Bainite in low-carbon low-alloy high strength steels, Trans. ISI Jap. 11 (1971), 250-259
7. Bhadeshia H.K.D.H., Edmonds D.V.: Acta Metall. A, vol. 28A, 1980, 1265
8. Zając S., Komenda J., Morris P., Dierickx P., Matera S., Penalba Diaz F.: Quantitative structure-property relationship for complex bainitic microstructures, 2005, Report EUR21235EN, Luxembourgh, Technical Steel Research, European Commision
9. Streicher-Clarke A.M., Speer J.G., Matlock D.K., De Cooman B.C., Williamson D.L.: Analysis of Lattice Parameter Changes Following Deformation of a 0.19C-1.63Si-1.59Mn Transformation Induced Plasticity Sheet Steel, Metall. Mater. Trans., A36 (2005) 4, 907-918
10. Cullity B.D., Stock S.R.: Elements of X-ray Diffraction, Pearson/Prentice Hall, Inc., (2001)
11. Pietrzyk M., Kuziak R.: Analysis of theoretical methods of evaluation of bainitic hardenability of steels, Proc. METAL 2013, Brno, 2013, e-book